JOURNAL OF APPLIED ELECTROCHEMISTRY 24 (1994) 917–922

Impedance measurements on some doped MnO_2 electrodes in H_2SO_4 electrolyte

B. D. DESAI*, F. S. LOBO, V. N. KAMAT DALAL

Department of Chemistry, Goa University, P.O. Bambolim – 403203, Goa, India

Received 19 April 1993; revised 8 February 1994

A.c. impedance behaviour of β-MnO_2 and doped β-MnO_2 electrodes in H_2SO_4 medium was assessed with a view to explaining the mechanism of the discharge behaviour of MnO_2 electrodes in 4 M H_2SO_4 electrolyte. The electrodes used in this work appear to be intermediate cases of planar and porous electrodes as the angles, θ, made by the low frequency part with the real axis are found to be in the range (30–60°). The Nyquist plots and the Randle plots tend to reinforce the observation made by Tye that the capacity yield is essentially diffusion controlled. The depression and flattening of semi-circles observed reveals a link with the heterogeneity of the planar electrode and with the porosity of the pitted electrode. The deviation from a 45° angle made by the low frequency part with the real axis may either be explained by the roughness of the electrode surface or the shallow pores on the surface of the electrodes; in other words due to the difference between the apparent and true surface areas. The double layer capacitance values of the electrodes seem to subsume adsorption capacitances and diffusion factors. Hence, the relative increase in magnitude. The electrodes appear to behave like planar electrodes when 10 μF is introduced into the circuit as a parallel capacitance since angles θ vary between 40–58°. The undoped β-MnO_2 electrode, as well as those prepared from Li–MnO_2, Ag–MnO_2, and I.C.8, appear to be planar electrodes.

1. Introduction

Impedance measurements for γ-MnO_2 powder dispersed in an electrolyte of resistivity 379 Ω cm were carried out by Atlung [1]. He gave an equivalent circuit in the form of an electrical transmission line to explain the process of diffusion in the electrolyte with filled channels between the particles. To improve the performance of batteries, fundamental studies in this regard are still necessary. Tests based on the impedance measurements of electrical storage cells have been devised for various cells [2, 3]. Karunathilaka *et al.* [4] investigated the impedance of the various components of the Leclanché cell and concluded that the effect of manganese dioxide is to depolarize the carbon electrode and the cell impedance becomes that associated with the zinc container. In the present work an attempt has been made to study the a.c. impedance behaviour of β-MnO_2 and doped β-MnO_2 samples with a view to explaining the mechanism of the discharge behaviour of the MnO_2 cathodes in 4 M H_2SO_4 electrolyte. The MnO_2 doped samples have proved to be good cathode materials in reserve primary batteries where 3–4 M H_2SO_4 is used as electrolyte [5]. Surprisingly the discharge duration is even better than that of International common samples electrolytic MnO_2 I.C.4 and I.C.8 which were used as reference samples. The doped samples performed well as cathode materials when the electrochemical evaluation was carried out in different electrolytes [6] such as (a) Leclanché (5 M NH_4Cl + 2 M $ZnCl_2$), (b) 25% $ZnCl_2$ and (c) 25% $ZnCl_2$ with additives (i.e. 2% LiCl + 1% NH_2SO_3H).

2. Experimental details

The doped manganese dioxides (β-MnO_2) were prepared by thermal decomposition (180 °C) of manganese nitrate in the presence of weighed quantities of NH_4VO_3, $Na_2WO_4.2H_2O$, $LiNO_3$, $AgNO_3$ and MoO_3. Valand's [7] procedure was followed and extended to other dopants. The salts used for doping were similar to those used by Rophael *et al.* [8]. All samples were prepared by thermal decomposition of an intimate mixture of $Mn(NO_3)_2.4H_2O$ and the dopant salt at 180 °C for five days. After decomposition the oxide was ground to pass 200 mesh sieve. The powder was washed with distilled water several times, except in the case of molybdenum and vanadium doped samples where a 7.5 N ammonia solution was added to the oxide and stirred for 30 min for the removal of unreacted molybdenum as ammonium molybdate and precipitated unoxidized manganous ions as manganous hydroxide. The oxides were then washed with water and dried at 110 °C to constant weight and stored over P_2O_5 in a dessicator. The quantities of reagents used for doping

* Author to whom correspondence should be addressed.

0021-891X

Table 1. Preparation, chemical analyses, chemical composition and reactivity of manganese dioxide samples

Sample	*Quantities of reagents used in the preparation of samples*	*Dopant*/%*	*MnO_2/%*	*Mn/%*	*x in MnO_{1+x}*	*Combined H_2O/% y'*	*Surface area (ZIA) /$m^2\,g^{-1}$*	*Crystallite size/nm (hkl 100)*
S0	200.8 g $Mn(NO_3)_2.4H_2O$	–	98.43	63.18	0.9846	0.20	8.75	27.7
S2	175.7 g $Mn(NO_3)_2.4H_2O$ + 10.08 g MoO_3	2.64 (Mo)	81.48	64.55	0.7977	3.10	24.50	27.4
S3	150.6 g $Mn(NO_3)_2.4H_2O$ + 0.864 g MoO_3	1.05 (Mo)	93.48	61.80	0.9559	1.10	26.25	12.0
S4	175.5 g $Mn(NO_3)_2.4H_2O$ + 0.1008 g MoO_3	0.12 (Mo)	95.40	65.92	0.9146	0.70	24.50	41.0
S5	200.8 g $Mn(NO_3)_2.4H_2O$ + 0.04 g MoO_3	0.03 (Mo)	96.70	64.02	0.9546	0.50	29.00	20.5
Li-1	200.8 g $Mn(NO_3)_2.4H_2O$ + 55.16 g $LiNO_3$	0.03 (Li)	99.65	62.14	1.0131	0.30	60.50	20.5
Li-2	200.8 g $Mn(NO_3)_2.4H_2O$ + 5.516 g $LiNO_3$	0.06 (Li)	97.94	63.18	0.9797	0.60	70.60	27.4
Ag-1	175.7 g $Mn(NO_3)_2.4H_2O$ + 1.189 g $AgNO_3$	1.02 (Ag)	87.10	56.31	0.9775	2.60	55.00	24.6
Ag-2	175.7 g $Mn(NO_3)_2.4H_2O$ + 11.8909 g $AgNO_3$	9.90 (Ag)	88.84	54.94	1.0210	1.80	59.50	33.6
W	200.8 g $Mn(NO_3)_2.4H_2O$ + 2.6388 g $Na_2WO_4.2H_2O$	3.05 (W)	94.04	60.43	0.9835	0.80	96.25	16.9
V	175.7 g $Mn(NO_3)_2.4H_2O$ + 8.1886 g NH_4Vo_3	5.30 (V)	82.02	59.06	0.8776	1.60	110.25	27.4
I.C.8	–	–	90.20	61.77	0.9229	2.42	79.52	–
I.C.4	–	–	88.75	59.88	0.9367	2.88	50.75	–

* Percentage dopant was estimated using AAS.

and the chemical analysis data is presented in Table 1. All chemicals used were of AR grade.

Impedance measurements using cathodes of MnO_2 containing different dopants like Mo, Ag, W, Li, V were recorded on a model 378 electrochemical impedance system (EG&G Princeton Applied Research) over a frequency range of 50 mHz to 100 kHz. A potentiostat for a.c. and d.c. potential control and current sensing and a lock-in amplifier (for frequency a.c. current and potential measurement) were used. All impedance measurements were carried out at 25 °C. The equivalent circuit is shown in Fig. 1. MnO_2 on preanodized lead (Pb) foil was used as the working electrode and placed in the centre of the cell. On one side of the working electrode a platinum electrode, of large surface area, was used as the counter electrode and SCE as reference electrode was placed on the other side. One side of the working electrode was exposed and a surface area not exceeding 3.5 cm^2 was used for impedance measurements. The other side of the cathode and the remaining surface was coated with a thin layer of lacquer. Separators were used between the electrodes. The electrolyte was 4 M H_2SO_4.

An attempt was also made to study the impedance behaviour of the MnO_2 samples by applying a potential bias of 0.1 and 0.3 V. It was, however, observed that disintegration/flaking of the cathode mix took place and it fell into the electrolyte, making the system unstable for impedance measurements. The modified equivalent circuit, after introduction of a parallel capacitance of 10 μF, is shown in Fig. 7. This was done to discover any change in the Nyquist plot, as this is indicative of changes in the electrode processes.

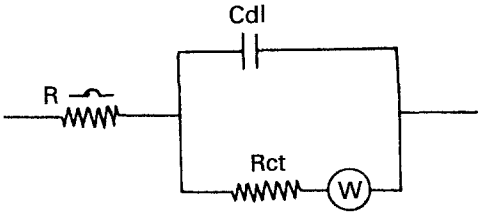

Fig. 1. Equivalent electronic circuit for a simple electrochemical cell.

3. Results and discussion

The dependence of the theoretical capacity of the electrodes on the square root of time is a clear indication that the capacity yield is essentially controlled by diffusion [15]. The Nyquist plots Figs 2–4 and the Randle's plots Figs 5 and 6 in the form of Z' against $\omega^{-1/2}$ and Z'' against $\omega^{-1/2}$ tend to reinforce the above observation [15]. The angles made by the low

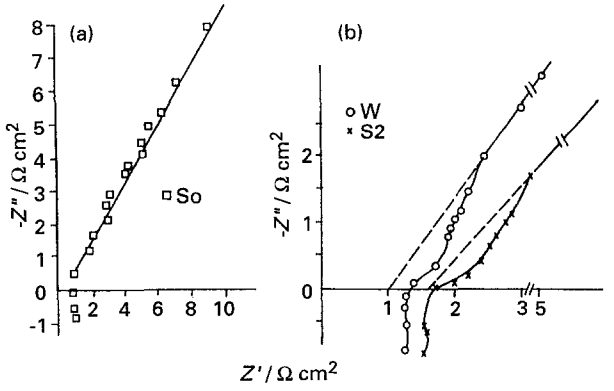

Fig. 2. Nyquist plots, $-Z''$ against Z' for: (a) S0 (□), undoped MnO_2 and (b) W (○), tungsten-doped MnO_2 and S2 (×), molybdenum-doped MnO_2.

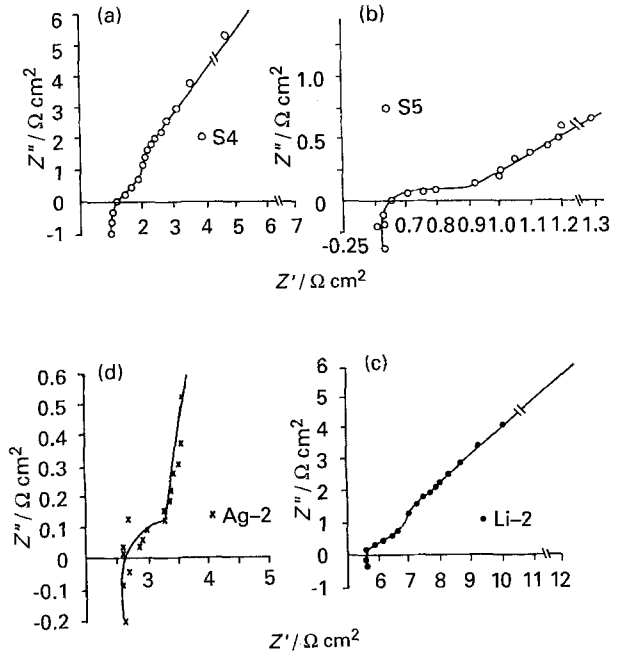

Fig. 3. Nyquist plots, $-Z''$ against Z' for: (a) S4 (○), molybdenum-doped MnO_2; (b) S5 (○), molybdenum-doped MnO_2; (c) Li-2 (•), lithium-doped MnO_2; (d) Ag-2 (×), silver-doped MnO_2.

frequency part with the real axis (i.e. Z') are found to be in the range (30–60°).

The variable range of this phase angle indicates that the electrodes used in this work were intermediate between planar and porous electrodes as the angle is neither 45° nor 22.5°. Most of the angles fall above 45° and very few below. De Levie [9], emphasizes the effect of a limited roughness on the impedance spectrum. This roughness causes the Warburg impedance to diverge from the 45° slope in the complex

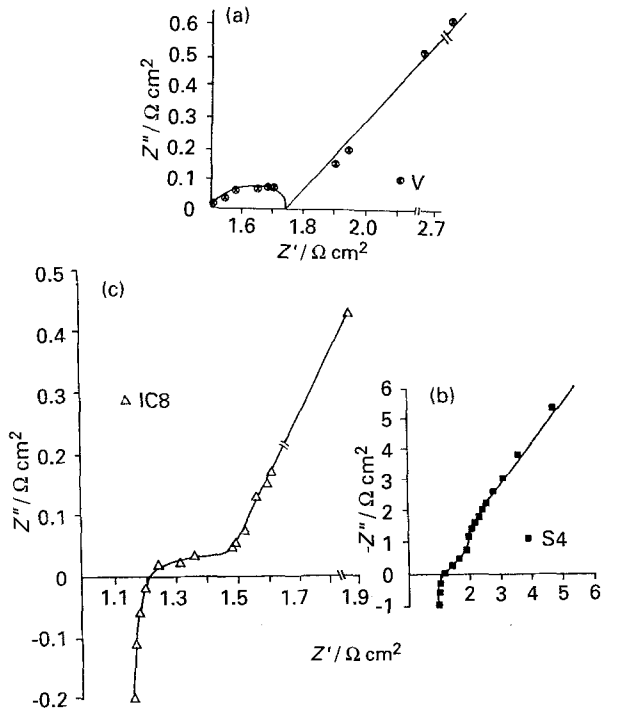

Fig. 4. Nyquist plots $-Z''$ against Z' for: (a) V (⊗), vanadium-doped MnO_2; (b) S4 (■), molybdenum-doped MnO_2; (c) I.C.8 (△).

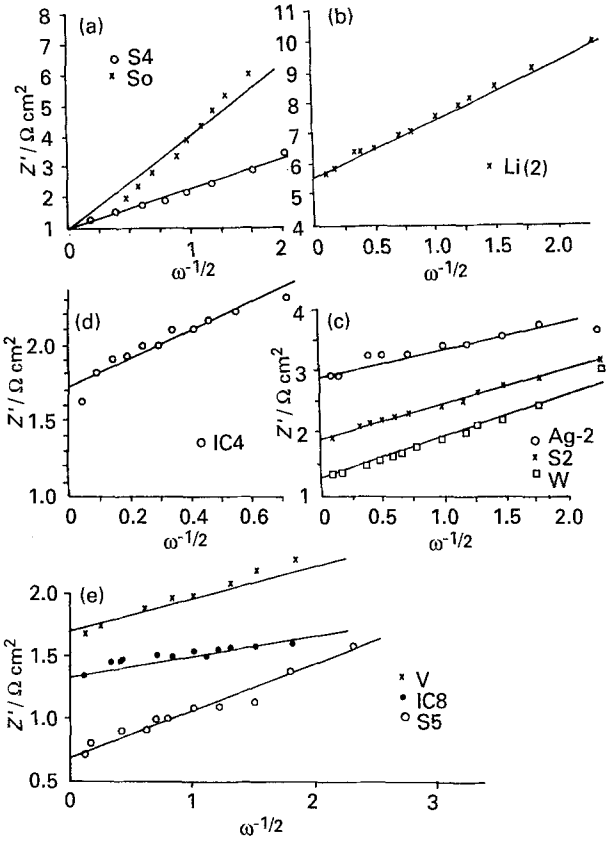

Fig. 5. Randle plots Z' against $\omega^{-1/2}$ for: (a) S4 (○), molybdenum-doped MnO_2 and S0 (×), undoped MnO_2; (b) Li-2 (×), lithium-doped MnO_2; (c) Ag-2 (○), silver-doped MnO_2, S2 (×), molybdenum-doped MnO_2 and W (□), tungsten-doped MnO_2; (d) I.C.4 (○); (e) V (×), vanadium-doped MnO_2, I.C.8 (•) and S5 (○), molybdenum-doped MnO_2.

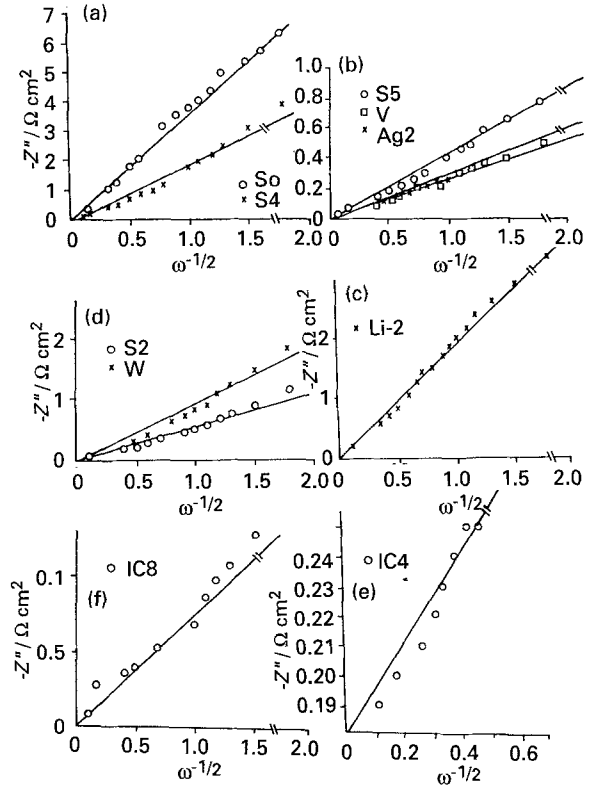

Fig. 6. Randle plot $-Z''$ against $\omega^{-1/2}$ for: (a) S0 (○), undoped MnO_2 and S4 (×), molybdenum-doped MnO_2; (b) S5 (○), molybdenum-doped MnO_2, V (□), vanadium-doped MnO_2 and Ag-2 (×), silver-doped MnO_2; (c) Li-2 (×), lithium-doped MnO_2; (d) S2 (○), molybdenum-doped MnO_2 and W (×), tungsten-doped MnO_2; (e) I.C.4 (○); (f) I.C.8 (○).

Table 2. Impedance data for MnO_2 samples

Sample	*DC potential/mV*	*Angle, θ/degree*	*R/Ω*	*Capacitance of double layer, C_{dl}/F*	*Charge transfer resistance, R_{ct}/Ω cm²*	*Warburg slope*	*Randle's slope*	*Warburg impedance, Z_w/Ω*
S0	1102	60.0	1.00	3.380	1.00	0.625	3.20	1.00
S2	1144	48.5	1.70	0.058	1.90	1.071	0.52	1.90
S4	1145	53.0	1.20	1.770	1.30	1.330	1.33	1.30
S5	1137	30.0	0.65	0.433	0.67	1.428	0.38	0.67
Ag-2	1097	80.0	2.60	0.251	2.90	0.833	0.42	2.90
Li-2	1161	41.0	5.50	1.810	5.60	1.200	1.90	5.60
V	1192	49.0	1.50	0.309	1.67	1.290	0.57	1.67
W	1147	54.5	1.30	0.940	1.25	1.250	0.62	1.25
I.C.8	1110	63.0	1.21	0.073	1.35	1.110	0.16	1.35
I.C.4	1222	73.0	1.00	0.150	1.82	0.316	1.00	1.82

plane to a limit of 22.5° for a completely porous electrode (infinite pore length). If there is interference from activation control, this may lead to lowering of θ from 45°. Karunathilaka *et al.* [16] also observed distortion in the Warburg slope if the pores are very shallow. In this work it was observed, with all the MnO_2 samples investigated, that a well defined open-circuit voltage (d.c. potential) was rapidly established and it remained constant up to the end of the electrical measurements. The open-circuit voltage also remained unaltered while standing for long periods. This observation is in agreement with the work of Karunathilaka *et al.* [10] on Leclanché cells. This is a satisfactory indication that the impedance measurements did not disturb the electrochemistry of the system. The values of the d.c. potential are presented in Table 2.

The data obtained from Nyquist plots i.e. Z' against Z'' and Randle plots are also given in Table 2. It is seen from Figs 2–4 that the semicircles are either depressed or flattened Nyquist plots. The depression is clearly seen in the vanadium doped sample (Fig. 4(a)). S5 and I.C.8 show flattening (see Figs 3(b) and 4(c)). This depression, or flattening, is indicative of mixed control of the electrode process, as well as being related to the heterogeneity of the planar electrode and also the porosity of the pitted electrode [10].

Hampson *et al.* [2], conclude that porosity affects the impedance of the electrodes at all frequencies and, in particular, it may lead to the impedance becoming inductive at high frequencies. In the present work an inductive loop at high frequencies is seen in the case of W, S2, S5, Li-2, S4, I.C.4, I.C.8, Ag-2, and S0 samples. The self-inductive nature of electrochemical power sources at high frequencies has already been observed by many workers [11–13]. Gutman [13] discussed this effect and concluded that, whenever the electrode system behaves as a negative resistance and furnishes energy to the measuring device, an inductive component is present.

The imaginary component of the cell impedance is cancelled out at a frequency close to 6.310 kHz in the case of S0, Ag-2, V, I.C.8, S4 and Li-2, whereas in the case of S2 the frequency is 10 kHz, in S5 it is 2.5 kHz, in W it is 3.980 kHz and in I.C.4 it is 15.8 kHz.

The Warburg slopes are presented in Table 2. I.C.4 gives the lowest slope, 0.3166, increasing gradually to 0.625 in the case of the undoped sample and 0.833 in the case of Ag-2. In the rest of the samples the slopes vary between 1.0 to 1.42. Reid and Loyselle [14] interpret the Warburg slope as an empirical parameter related qualitatively, rather than quantitatively, to the diffusion resistance where a higher slope signifies a slower rate of diffusion and a low slope a more rapid rate of diffusion. The present data were inconclusive. The relatively large double layer capacitance cell values obtained in this work appear to include, not merely the values of cell, but also those of adsorption capacitances and diffusion factors [14].

According to Karunathilaka *et al.* [16], the high surface area of MnO_2 ensures that the nominal MnO_2 electrolyte characteristic charge transfer resistance and Warburg coefficient are both small, and the corresponding double layer capacitance very large. Table 2 reveals the large values of double layer capacitance and low values of charge transfer resistance (R_{ct} in Ωcm^2) in the range 1.0–2.9 Ωcm^2 except in Li-2 where it is 5.6 Ωcm^2. The surface area of the MnO_2 samples are in the range 8.75 $m^2 g^{-1}$ to 110.25 $m^2 g^{-1}$ (Table 1). The R_{ct} values reported by Karunathilaka *et al.* are in the range 2.42–2.69 Ωcm^2 in the case of undischarged Leclanché cells. R_{ct} and C_{dl} values obtained here appear reasonable. The large C_{dl} values may also be due to the difference between the true and the apparent surface area, as indicated by De Levie [9].

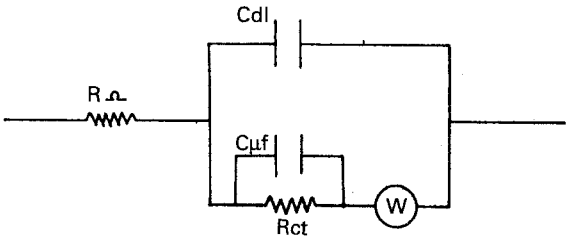

Fig. 7. Equivalent electronic circuit with a capacitance C in parallel with R_{ct}.

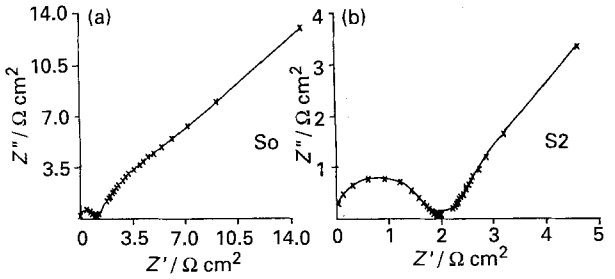

Fig. 8. Nyquist plots, $-Z''$ against Z' for: (a) S0 (×), undoped MnO_2; (b) S2 (×), molybdenum-doped MnO_2.

An attempt to calculate R_{ct} using I_0 from a Tafel plot was made using the equation

$$R_{ct} = \frac{RT}{nFI_0} \quad (1)$$

where R_{ct} is the charge transfer resistance and other symbols have their usual meaning.

Unfortunately, the R_{ct} values calculated from Equation (1) do not agree with those obtained by the impedance method. This is probably due to the reference and counter electrodes being different. The exposed electrode area is also different.

The I_0 values of Ag-1, Ag-2, Li-2, and S3 are significantly higher (Table 4) and it was expected, therefore, that the Warburg slopes should be correspondingly lower, if the contention of Ried and Loyselle [14] is tenable. However, there does not appear to be a direct correlation between these two parameters. Nevertheless, Ag-2, Li-2, S5 and V–MnO_2 exhibit an overall superiority in terms of their percentage utilization, milliampere hours obtained and service rendered in different discharge regimes in both H_2SO_4 and $ZnCl_2$ electrolytes [5, 6]. The Warburg slopes, however, are not significantly low as expected, except in the case of Ag-2 and I.C.4.

With a parallel capacitance added, the modified equivalent circuit is shown in Fig. 7. A 10 μF capacitor was added to the circuit containing samples S0, S2, S3, S4, S5, Li-2, Ag-2, W, V and I.C.8. From

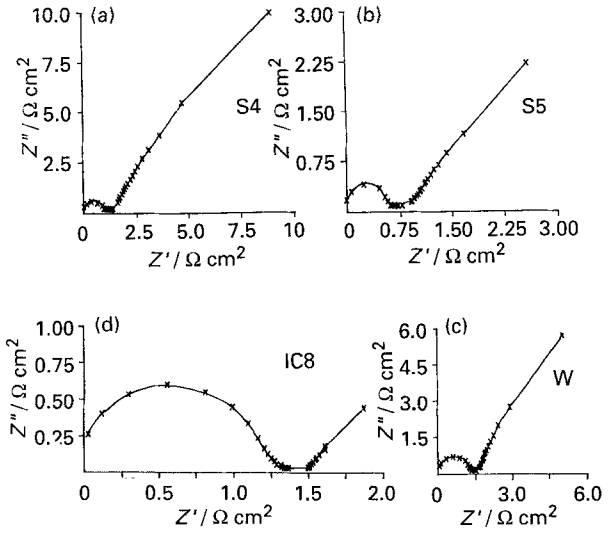

Fig. 9. Nyquist plots, $-Z''$ against Z' for: (a) S4 (×), molybdenum-doped MnO_2; (b) S5 (×), molybdeum-doped MnO_2; (c) W (×), tungsten-doped MnO_2; (d) I.C.8 (×).

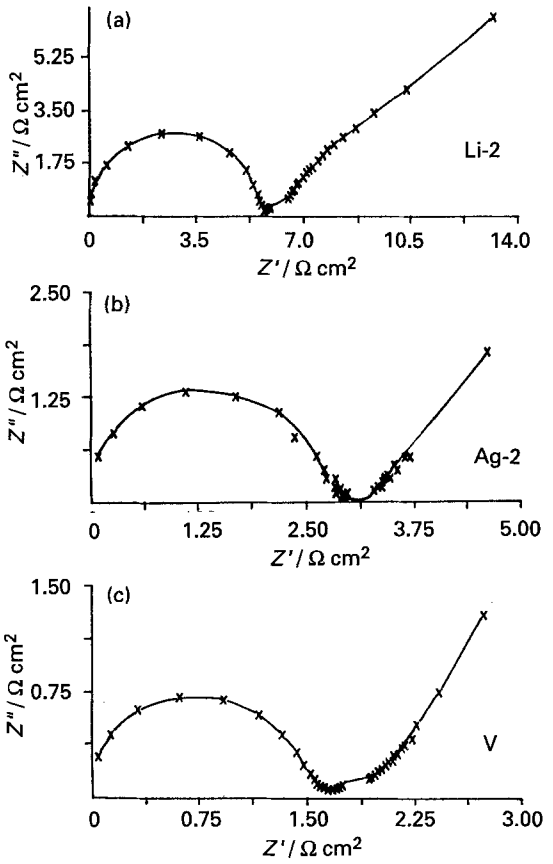

Fig. 10. Nyquist plots, $-Z''$ against Z' for: (a) Li-2 (×), lithium-doped MnO_2; (b) Ag-2 (×), silver-doped MnO_2; (c) V (×), vanadium-doped MnO_2.

the Nyquist plots Z' against $-Z''$ presented in Figs 8–11, it is seen that the semicircle is complete only in the case of undoped β-MnO_2 i.e. the S0 sample, whereas in the case of the other samples the semicircle touches the imaginary component ($-Z''$) above zero and, hence, the phase angle in all other samples, except S0, could not be recorded directly. The semicircle was manually completed and the phase angle found. The Warburg component is seen in all cases and the angle θ, made by the linear tail portion with the real axis, is presented in Table 3. The electrodes behave like planar electrodes when 10 μF is introduced into the circuit, as the angle, θ, made by the linear tail portion with the real axis varies between 40° and 58°. This is consistent with the observation of De Levie [9]. Comparing these angles (θ) with those of the original samples (Table 2), it is seen

Table 3. Impedance data for MnO_2 samples with 10 μF in circuit

Sample	*Phase angle, δ/degrees*	*θ/degree*	*$R_p + R/\Omega$*
S0	61.5	40	0.88
S2	59.0	50	1.80
S4	57.5	52	1.25
S5	61.0	50	0.56
Li-2	67.5	42	5.68
Ag-2	64.0	49	2.96
W	52.0	57	1.50
V	62.0	58	1.68
I.C.8	66.0	47	1.30

Table 4. Polarization characteristics of MnO_2 samples

Sample	*Exchange current density, I_0/mA cm^2*	*Tafel constants* *a*	*b*	*Transfer coefficient*
S0	0.2345	−0.0373	−0.0592	0.9994
S2	1.221	0.0051	−0.5928	0.9996
S3	2.225	0.0250	−0.0592	0.9997
S4	1.010	0.00025	−0.0592	0.9997
S5	1.1618	0.0038	−0.0592	0.9996
Ag-1	4.9530	0.0411	−0.0592	0.9998
Ag-2	6.3598	0.0476	−0.0592	0.9999
Li-1	0.2232	−0.0386	−0.0592	0.9995
Li-2	3.158	0.0296	−0.0592	0.9995
V	0.2232	0.0064	−0.0592	0.9997
W	1.2840	0.0064	−0.0592	0.9997

that there is a change except in the case of the Li-2 sample, indicating that the addition of 10 μF to the circuit has a pronounced effect on θ. The values of polarization resistance, R_p, which is in fact the charge transfer resistance R_{ct}, is at variance with those obtained from the Randle plot. Charge transfer and mass transfer regions seem to be more clearly delineated in these Nyquist plots (Figs 8–10).

References

[1] S. Atlung and T. Jacobsen, *Electrochim. Acta* **21** (1976) 575.
[2] N. A. Hampson, S. A. G. R. Karunathilaka and R. Leek, *J. Appl. Electrochem.* **10** (1980) 3.
[3] J. Euler and K. Dehmelt, *Ber. Bunsenges. Phys. Chem.* **61** (1957) 1200.
[4] S. A. G. R. Karunathilaka, N. A. Hampson, R. Leek and T. J. Sinclair, *J. Appl. Electrochem.* **10** (1980) 603.
[5] B. D. Desai, F. S. Lobo and V. N. Kamat Dalal, accepted for publication in *J. Power Sources.*
[6] B. D. Desai, F. S. Lobo and V. N. Kamat Dalal, accepted for publication in *J. Power Sources.*
[7] T. Valand, *J. Power Sources* **1** (1976/77) 65.
[8] M. W. Rophael, T. A. Bibawy, L. B. Khalil and M. A. Malati, *Chemistry and Industry*, No. 1, 6 Jan. (1979) p. 27.
[9] R. De Levie, *Adv. Electrochem Eng.* **6** (1967) 329.
[10] S. A. G. R. Karunathilaka, N. A. Hampson, R. Leek and T. J. Sinclair, *J. Appl. Electrochem.* **10** (1980) 604, 799.
[11] E. Willihnganz, *J. Electrochem. Soc.* **102** (1955) 99.
[12] J. J. Lander and E. E. Nelson, *ibid.* **107** (1960) 723.
[13] F. Gutman, *ibid.* **112** (1965) 94.
[14] M. A. Reid and P. L. Loyselle, *J. Power Sources* **36** (1991) 285.
[15] F. L. Tye, 'Electrochemical Power Sources' *in* 'Primary Batteries for Civilian Use' (edited by M. Barak), Peter Peregrinus, London (1980) p. 92.
[16] S. A. G. R. Karunathilaka, N. A. Hampson, R. Leek and T. J. Sinclair, *J. Appl. Electrochem.* **10** (1980) 357.